Supporting Information

Ultrafast Catalyst-Free Growth of Graphene Film on Glass Assisted by Local Fluorine Supply

Yadian Xie,[†] Ting Cheng,[†,#] Can Liu,[§] Ke Chen,[†,‡] Yi Cheng,[†] Zhaolong Chen,[†] Lu Qiu,[#] Guang Cui,[†] Yue Yu,[†] Lingzhi Cui,[†] Mengtao Zhang,[†] Jin Zhang,[†,¶] Feng Ding,*[,#] Kaihui Liu,*[,§,¶] and Zhongfan Liu*[,†,¶]

[†]Center for Nanochemistry, Beijing National Laboratory for Molecular Sciences, College of Chemistry and Molecular Engineering, Academy for Advanced Interdisciplinary Studies, Peking University, Beijing 100871, China

[§]State Key Laboratory for Mesoscopic Physics, Collaborative Innovation Center of Quantum Matter, School of Physics, Academy for Advanced Interdisciplinary Studies, Peking University, Beijing 100871, China

[#]Centre for Multidimensional Carbon Materials, Institute for Basic Science, School of Materials Science and Engineering, Ulsan National Institute of Science and Technology, Ulsan 44919, Korea

[¶]Beijing Graphene Institute (BGI), Beijing 100095, China

[‡]Institute of Micro/Nano Photonic Materials and Applications, School of Physics and Electronics, Henan University, Kaifeng 475004, China

*To whom correspondence should be addressed. E-mail: zfliu@pku.edu.cn, khliu@pku.edu.cn, f.ding@unist.ac.kr

Figure S1: Measurement of the gap between the metal fluoride and quartz surfaces.

The cross section of the freely placed quartz on BaF_2 substrate can be observed directly by an optical microscope. The narrow gap between the two surfaces is only ~30 μm, which provides a confined space for the fluorine released from the fluoride at the growth temperature of ~1,000 ℃.

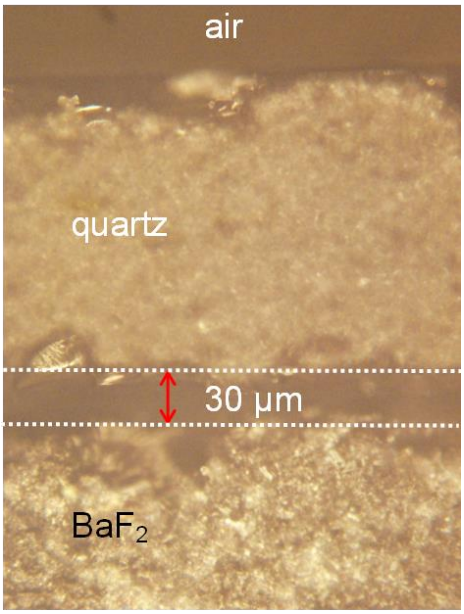

Figure S1. Typical optical image for the cross section of quartz on a BaF_2 substrate.

Figure S2: Graphene growth on quartz supported by other metal fluorides and non-fluorides

We grew graphene on quartz glass assisted by different fluorides and non-fluorides. Growth supported by CaF_2 and MgF_2 substrates showed the full coverage of graphene film on quartz glass in 5 min. But for the growth supported by sapphire and SiO_2/Si, no graphene domain is observed on the quartz glass within 5 min.

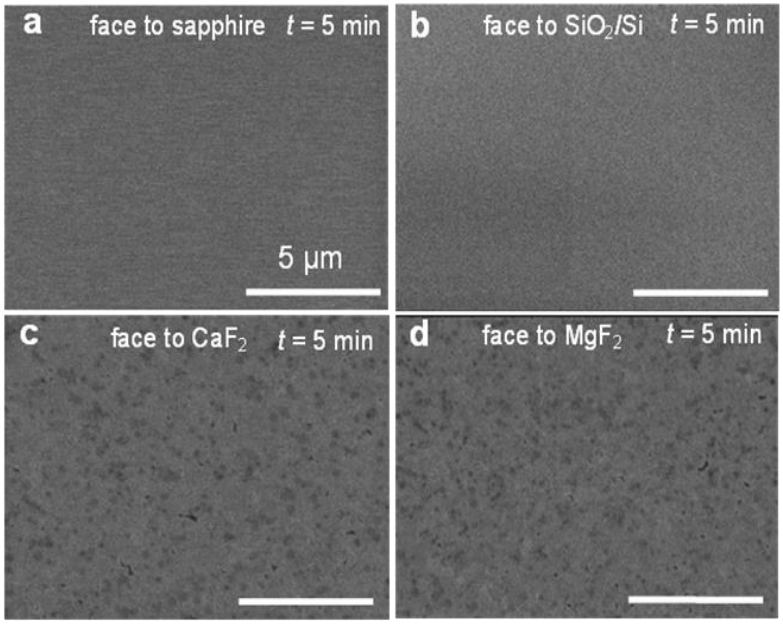

Figure S2. SEM images of graphene grown on the surface of ST-cut quartz glass supported by **(a)** sapphire, **(b)** SiO_2/Si substrate, **(c)** CaF_2 and **(d)** MgF_2.

Figure S3: Graphene growth on SiO_2/Si substrate assisted by local-fluorine-supply method

The graphene film on SiO_2/Si substrate assisted by the local-fluorine-supply method reached full coverage in just 5 min as well (Figure S3a). The 2D/G peak intensity in Raman spectrum (Figure S3b) demonstrates the graphene film mainly consists of monolayers. Our results showed the universality of the local-fluorine-supply method in graphene growth on dielectric substrates.

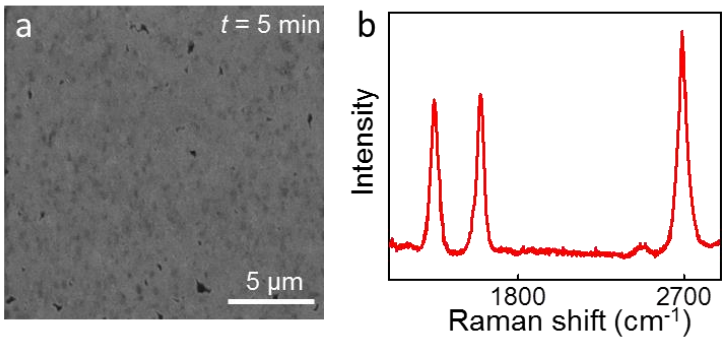

Figure S3. (a) SEM image and **(b)** Raman spectrum of graphene grown on SiO_2/Si substrate assisted by fluorine in 5 min.

Figure S4: High-resolution transmission electron microscopic (HRTEM) images of different graphene samples on quartz glass

A large number of HRTEM images of different graphene quartz glass samples confirmed that the graphene films are primarily monolayers.

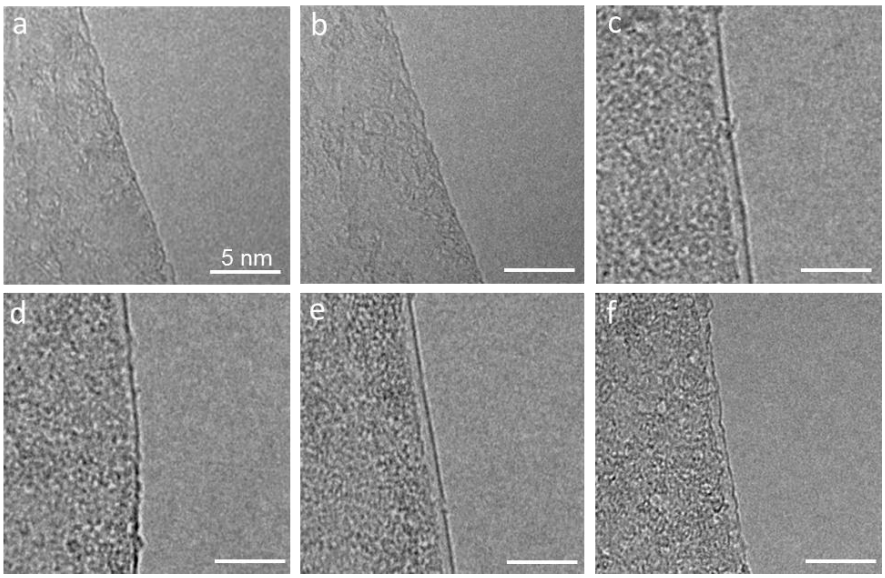

Figure S4. HRTEM images of monolayer graphene film.

Figure S5: Atomic Force Microscope (AFM) images of graphene films transferred onto SiO_2/Si substrate.

The thickness of graphene was checked by AFM as shown in Figure S5, which further illustrated that the as-grown graphene films in 5 min are primarily monolayers.

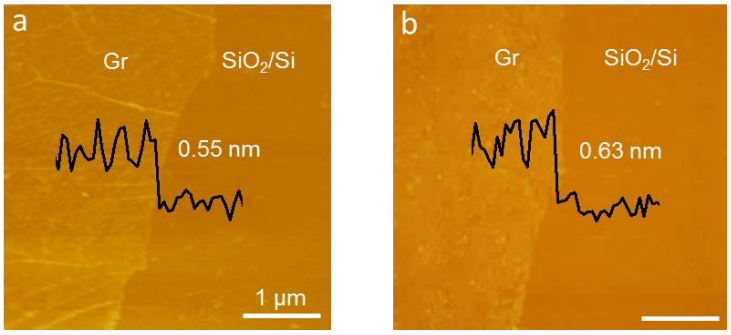

Figure S5. AFM images of the edge of graphene films.

Figure S6: Raman mapping of the as-grown graphene film

Raman mapping also demonstrates the quality and uniformity of the graphene film which was transferred onto a 300 nm SiO_2/Si substrate, as shown in Figure S6a (the darker region is the graphene sample). As shown in Figure S6b-e, the slight colour variation in the D, G, 2D mode and I_{2D}/I_G mapping indicates the uniformity of the graphene film.

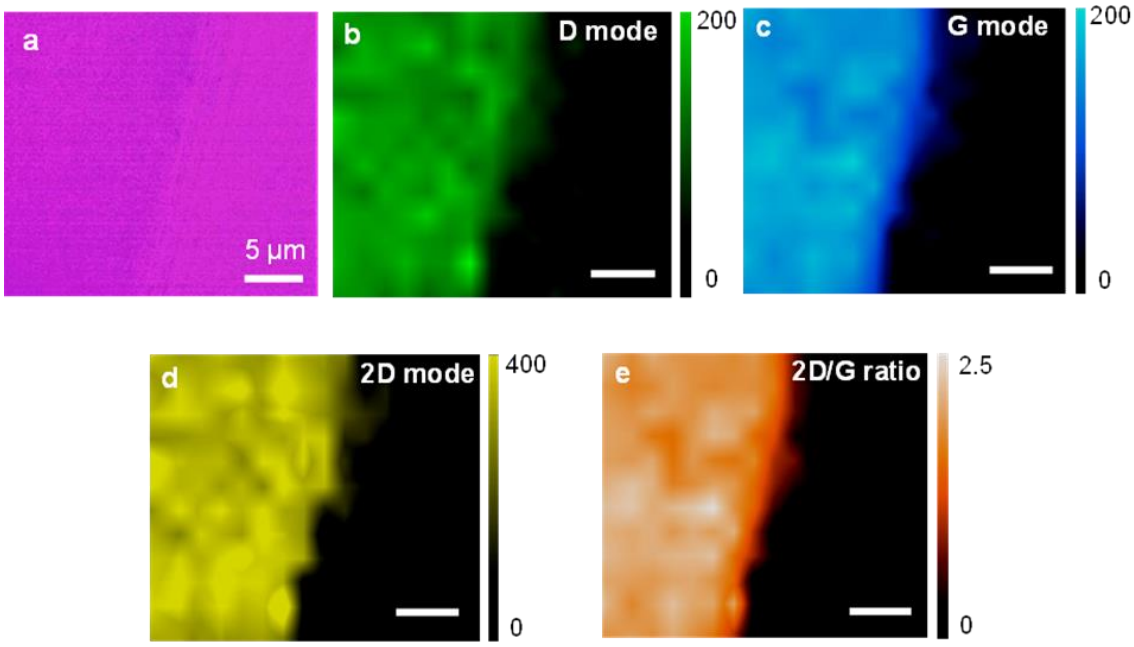

Figure S6. Raman mapping of graphene film. **(a)** Optical image of the graphene film. **(b-d)** The corresponding D, G, and 2D mode mapping**. (e)** I_{2D}/I_G ration mapping.

Figure S7: The quality of graphene films grown without fluorine (grown by quartz confined)

The quality of graphene films grown without fluorine assistance was checked by Raman spectroscopy (Figure S7a), and the graphene films are mainly monolayers demonstrated by 2D/G peak intensity. In addition, HRTEM images illustrated that most of the samples are primarily monolayers with small few-layer regions (Figure S7b-c), and the selected area electron diffraction (SAED) showed the polycrystalline structure of graphene film grown without fluorine assistance (Figure S7b). These characteristics are all corresponding with that of graphene grown by the local-fluorine-supply method.

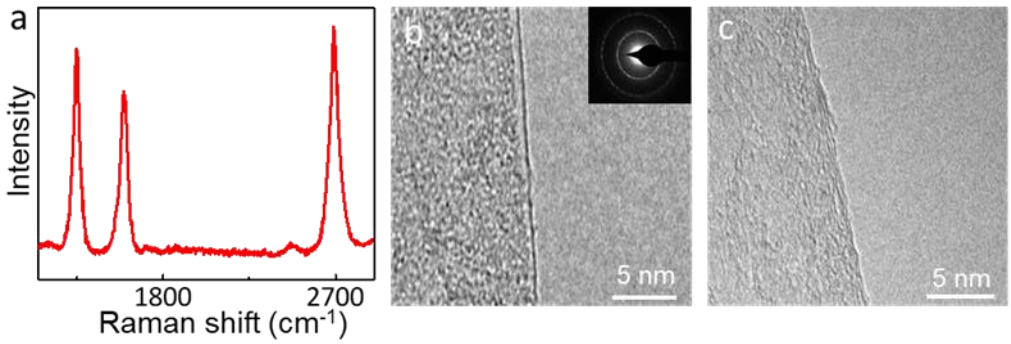

Figure S7. Quality of graphene film grown without fluorine (grown by quartz confined). **(a)** A representative Raman spectrum of graphene film. **(b-c)** HRTEM images of (b) monolayer and (c) multilayer regions. The inset is the corresponding SAED.

Figure S8: X-ray photoelectron spectroscopy (XPS) of graphene on quartz glass

We find the absence of F 1s peak in the survey of the XPS spectrum as shown in Figure S8a. In addition, according to the C 1s peak analysis, there are no C-F bonds formed in the as-grown graphene film. Therefore, we can conclude that there is no fluorine doping in the graphene films.

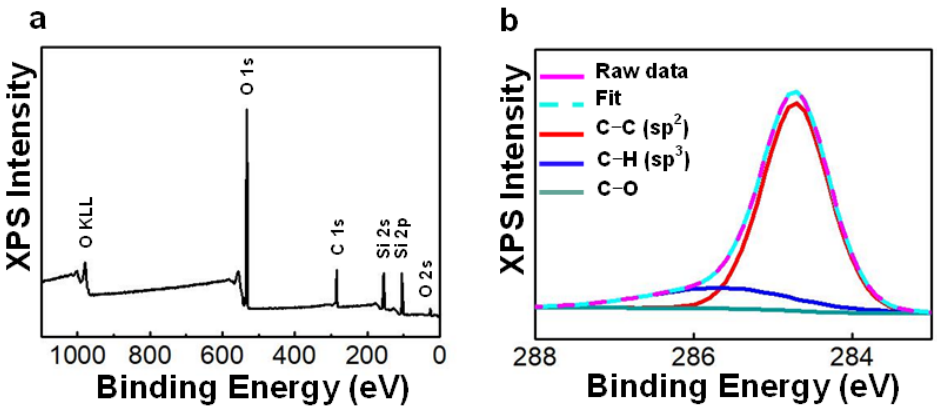

Figure S8. (a) Representative survey XPS spectrum of the fluorine assisted graphene glass. **(b)** C 1s XPS spectrum displayed the absence of C-F bonds, indicating the high quality of graphene glass without fluorine doping.

Figure S9: Comparison of utilization efficiency of CH_4 with fluorine and without fluorine by Mass Spectroscopy (MS)

The measurements of mass spectroscopy were employed to analyze the exhaust of the CVD system. The results of MS (Figure S9) indicated that utilization efficiency of CH_4 with fluorine assisted is about 15% higher than that of without fluorine. However, the concentration of F and CH_3F in the CVD system is too small to be detected by MS.

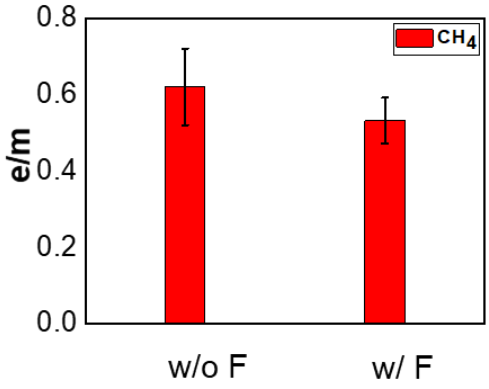

Figure S9. Comparison of utilization efficiency of CH_4 by using mass spectroscopy.

Figure S10: The energy profile of CH_3F formation

For the formation of CH_3F, the reaction barrier is only 0.66 eV and the reaction is highly exothermic, therefore, we can expect a considerable amount of CH_4 molecules was converted into CH_3F molecules in the narrow gap, as shown in Figure S10.

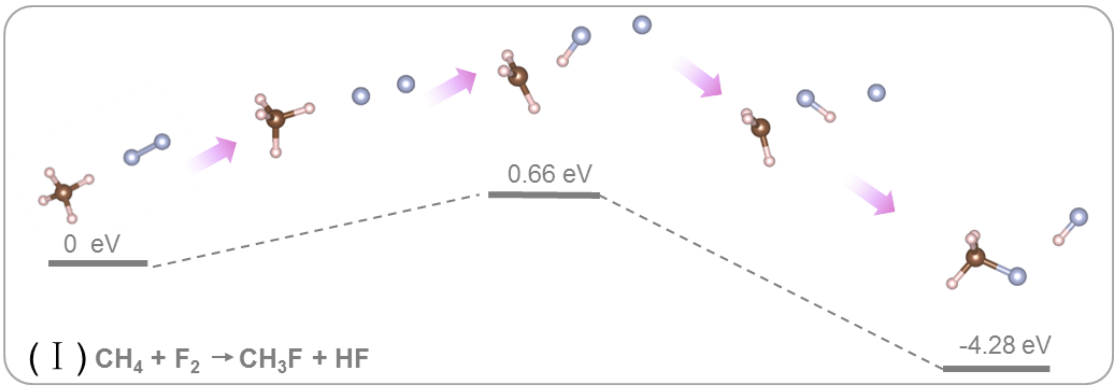

Figure S10. The formation of CH_3F in gas phase and the corresponding energy profile.

Figure S11: The first step for CH_3F reacting with graphene edge

The attachment of carbon atoms to graphene edge by the collision of gas phase molecules with the graphene edge is a necessary step for the graphene growth. We firstly assume that feedstock methane could be carbon precursor candidate to decompose and directly involved into the graphene edge growth, the entire process is shown in Figure S11. From left to right in this figure successively are initial, transition and final states.

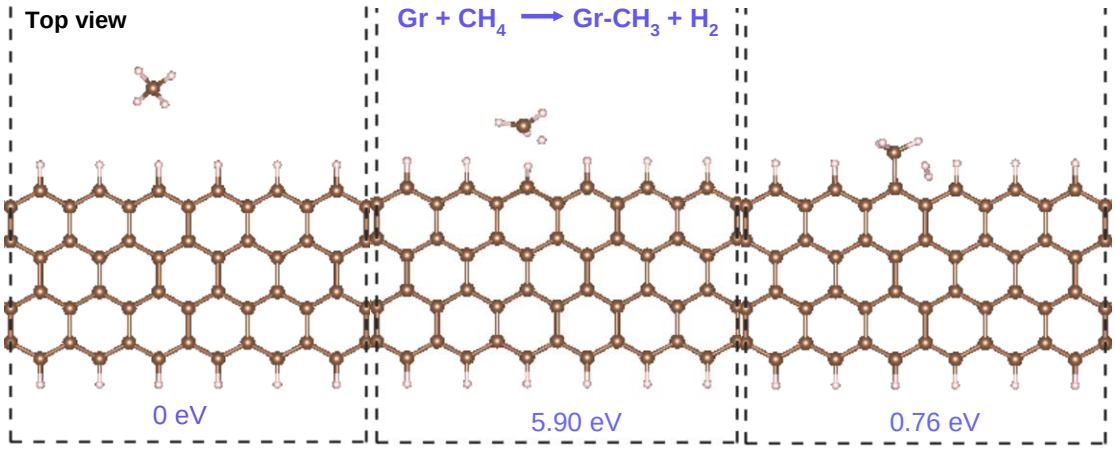

Figure S11. The calculation model of first step for CH_4 attaching to graphene edge. From left to right in this figure successively are initial, transition and final states.

Figure S12: The third step for CH_3F reacting with graphene edge

For CH_3F incorporation at the growth edge, the last route is a two-step reaction with two hydrogen atoms separately scratched, as shown in Figure S12. And the according relative energy is shown below the calculation model.

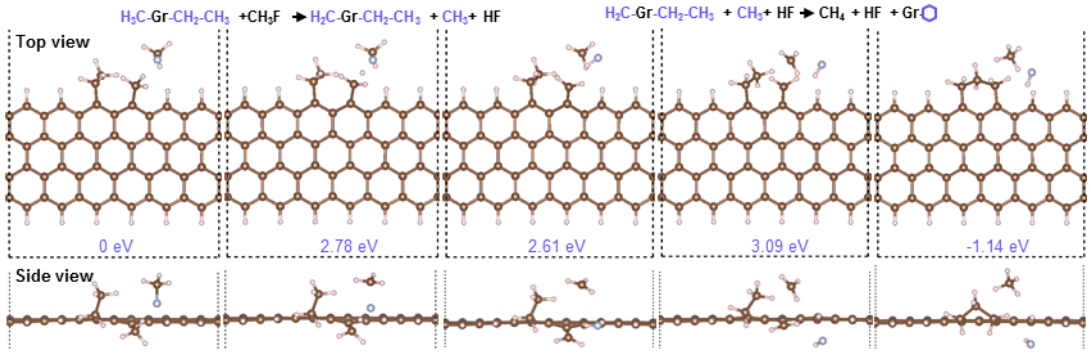

Figure S12. The concrete reaction process of third step for CH_3F attaching to graphene edge, composed of two steps. The according relative energy is shown in the calculation model.

Supporting Table 1. Reported growth time to realize a full-coverage graphene film on insulating substrates.

Table S1 Reported growth time to realize a full-coverage graphene film on insulating substrates.	
Group	**Growth time (min)**
Yuegang Zhang [1]	420
Xiaoming Xie [2]	360
Yunqi Liu [3]	240
Zhongfan Liu [4]	180
Hee Cheul Choi [5]	120
Zhongfan Liu [6]	75
This work	5

Supporting Method: Density functional theory calculation.

All the calculations above were performed with the Vienna *ab*-initio Simulation Package [7,8] with density functional theory using the method of the project augmented wave[9]. The exchange and correlation potentials were treated by the Perdrew-Burke-Ernzerhof (PBE) functional within the generalized gradient approximation (GGA)[10]. 400 eV was taken as energy cutoff, and we fully relaxed all the structures considering to let both the energy and force converge to 10^{-4} eV and 0.02 eV/ Å, respectively. The unit cell of slab models is 14.75 Å × 30.00 Å for the zigzag graphene nanoribbons. To avoid interaction between the adjacent unit cell, a vacuum layer along the z direction was kept as large as 14 Å. Unless specified, spin-polarization was used in all the calculations to fully include the effects of edge and small molecules. The energy barrier of each reaction step was studied by using the climbing image nudged elastic band (CI-NEB) approach [11].

References

(1) A. Ismach, C. Druzgalski, S. Penwell, A. Schwartzberg , M. Zheng, A. Javey, B. Jeffrey, Y. Zhang. Direct Chemical Vapor Deposition of Graphene on Dielectric Surfaces. *Nano Lett.* **2010**,*10*, 1542-1548.

(2) S. Tang, G. Ding, X. Xie, J. Chen, C. Wang, X. Ding, F. Huang, L. U. Wei, M. Jiang. Nucleation and Growth of Single Crystal Graphene on Hexagonal Boron Nitride. *Carbon* **2012**, *50*, 329-331.

(3) C. Jianyi, G. Yunlong, W. Yugeng, H. Liping, X. Yunzhou, G. Dechao, W. Bin, L. Birong, Y. Gui, L. Yunqi. Two-Stage Metal-Catalyst-Free Growth of High-Quality Polycrystalline Graphene Films on Silicon Nitride Substrates. *Adv. Mater.* **2013**, *25*, 992-997.

(4) J. Sun, Z. Chen, L. Yuan, Y. Chen, J. Ning, S. Liu, D. Ma, X. Song, M. K. Priydarshi, A. Bachmatiuk. Direct Chemical-Vapor-Deposition-Fabricated, Large-Scale Graphene Glass with High Carrier Mobility and Uniformity for Touch Panel Applications. *ACS Nano* **2016**, *10*, 11136-11144.

(5) H. J. Song, M. Son, C. Park, H. Lim, M. P. Levendorf, A. W. Tsen, J. Park, H. C. Choi. Large Scale Metal-Free Synthesis of Graphene on Sapphire and Transfer-Free Device Fabrication. *Nanoscale* **2012**, *4*, 3050-3054.

(6) Z. Chen, B. Guan, X.-d. Chen, Q. Zeng, L. Lin, R. Wang, M. K. Priydarshi, J. Sun, Z. Zhang, T. Wei. Fast and Uniform Growth of Graphene Glass Using Confined-Flow Chemical Vapor Deposition and Its Unique Applications. *Nano Res.* **2016**, *9*, 3048-3055.

(7) G. Kresse, J. Furthmüller. Efficiency of *ab*-initio Total Energy Calculations for Metals and Semiconductors Using A Plane-Wave Basis Set. *Comp. Mater. Sci.* **1996**, *6*, 15-50.

(8) G. Kresse, J. Furthmüller. Efficient Iterative Schemes for *ab*-initio Total-Energy Calculations Using A Plane-Wave Basis Set. *Phys. Rev. B.* **1996**, *54*, 11169.

(9) J. P. Perdew, K. Burke, M. Ernzerhof. Generalized Gradient Approximation Made Simple. *Phys. Rev. Lett.* **1996**, *77*, 3865.

(10) G. Kresse, D. Joubert. From Ultrasoft Pseudopotentials to the Projector Augmented-Wave Method. *Phys. Rev. B.* **1999**, *59*, 1758.

(11) G. Henkelman, B. P. Uberuaga, H. Jónsson. A Climbing Image Nudged Elastic Band Method for Finding Saddle Points and Minimum Energy Paths. *J. Chem. Phys.* **2000**, *113*, 9901-9904.